Extracellular Vesicles Derived from Glioblastoma Promote Proliferation and Migration of Neural Progenitor Cells via PI3K-Akt Pathway

Jiabin Pan
Tongji University Tenth People's Hospital: Shanghai Tenth People's Hospital
Shiyang Sheng
Tongji University Tenth People's Hospital: Shanghai Tenth People's Hospital
Ling Ye
Tongji University Tenth People's Hospital: Shanghai Tenth People's Hospital
Yizhao Ma
Tongji University Tenth People's Hospital: Shanghai Tenth People's Hospital
Lisha Qiu
Tongji University Tenth People's Hospital: Shanghai Tenth People's Hospital
Zhaohuan Fan
Tongji University Tenth People's Hospital: Shanghai Tenth People's Hospital
Yi Wang
Tongji University Tenth People's Hospital: Shanghai Tenth People's Hospital
Xiaohuan Xia
Tongji University Tenth People's Hospital: Shanghai Tenth People's Hospital
Yunlong Huang
University of Nebraska Medical Center College of Medicine
Jialin Zheng (jialinzheng@tongji.edu.cn)
Tongji University https://orcid.org/0000-0003-2286-0151

Research

Keywords: Glioblastoma, Extracellular vesicles, Neural progenitor cells, Proliferation, Migration, PI3K, Akt

Posted Date: January 28th, 2021

DOI: https://doi.org/10.21203/rs.3.rs-153837/v1

Version of Record: A version of this preprint was published at Cell Communication and Signaling on January 12th, 2022. See the published version at https://doi.org/10.1186/s12964-021-00760-9.

Abstract

Background

Glioblastomas are lethal brain tumors under the current combinatorial therapeutic strategy that includes surgery, chemo- and radio-therapies. Extensive changes in the tumor microenvironment is a key reason for resistance to chemo- or radio-therapy and frequent tumor recurrences. Understanding the tumor-nontumor cell interaction in TME is critical for developing new therapy. Glioblastomas are known to recruit normal cells in their environs to sustain growth and encroachment into other regions. Neural progenitor cells (NPCs) have been noted to migrate towards the site of glioblastomas, however, the detailed mechanisms underlying glioblastoma-mediated NPCs' alteration remain unkown.

Methods

We utilized two classic glioblastoma cell lines, U87- and A172, and collected EVs in the culture medium of those two lines. Mouse NPCs (mNPCs) were co-cultured with U87- or A172-derived EVs. EVs-treated mNPCs' prolifeartion and migration were examined. Proteomic analysis and western-blot were utilized to identify the underlying mechanisms of glioblastoma EVs-induced alterations in mNPCs.

Results

We show that glioblastoma cell lines U87- and A172-derived EVs dramatically promoted NPCs proliferation and migration. Mechanistic studies identify that EVs achieve their functions via activating PI3K-Akt-mTOR pathway in recipient cells. Inhibiting PI3K-Akt reversed the elevated prolfieration and migration of glioblastoma EVs-treated mNPCs.

Conclusion

Our findings demonstrate that EVs play a key role in intercellular communication in tumor microenvironment. Inhibition of the tumorgenic EVs-mediated PI3K-Akt-mTOR pathway activation might be a novel strategy to shed light on glioblastoma therapy.

Background

Glioblastomas are the most malignant gliomas (grade IV glioma) that contain a large proportion of dividing tumor cells nourished by ample and abnormal blood supply [1, 2]. They are highly infiltrative and invade other brain regions. Although surgery, radiation, and chemotherapy are developed for treating glioblastoma, no cure is available and the standard care for glioblastoma remains almost unchanged for nearly 20 years with a median life expectancy of 15 months from the time of diagnosis to death [3]. Given that, new insights on glioblastoma tumor cells and their surrounding cells are in urgent need for the development of new therapy.

Invasive growth of glioblastomas that depletes a thorough tumor resection and extensive changes in the tumor microenvironment (TME) are main reasons for observed resistance to current therapy and concomitant recurrence [4–6]. Glioblastomas are known to have the capacity to recruit and alter the phenotypes of normal cells in their environs to sustain growth and encroachment into other regions [7]. Numerous forms of cell-cell communication are utilized by glioblastomas to “hijack” cells in the TME to promote tumor progression [3–5]. These routes include direct secretion of soluble factors, exchange of proteins and molecules via gap junctions, and transfer cellular contents via extracellular vesicles (EVs) [8]. Via these routes, glioblastomas alter immune cell function, sustain tumor vasculature, cause neurotoxicity, and alter astroglia phenotypes. Formidably, a dominant proportion of surrounding cells further provide feedback to potentiate glioblastoma aggressiveness via this crosstalk [9, 10].

Neural progenitor cells (NPCs) have been noted to migrate towards the site of glioblastomas *in vitro* under the influence of chemoattractant secreted by glioblastoma tumor cells [11, 12]. However, the specific mechanism of communication between glioblastoma cells and neural progenitor cells remains unknown. EVs are small lipid bilayer vesicles budding from cell plasm [13–15] or budding off the tips of nanotubes [16] that play as essential intercellular communicators [17]. Our previous work demonstrated that EVs retain certain properties of their donors and able to confer donor properties to recipient cells [18]. Therefore, we hypothesized that glioblastoma-derived EVs may retain the tumor properties that altering the phenotype and function of surrounding NPCs. To test this premise, we utilized two classic glioblastoma cell lines, U87- and A172, and collected EVs in the culture medium of those two lines. Our results suggested that EVs derived from both lines significantly promoted proliferation and migration of NPCs. Next, proteomics and western blot analyses identified PI3K-Akt pathway as a key one that is enriched in glioblastoma-derived EVs and activated in EVs recipient cells in the meantime. The positive effects of glioblastoma-derived EVs on proliferation and migration of NPCs were further abrogated when recipient cells were treated with Wortmannin, a PI3K inhibitor [19], which, confirmed PI3K-Akt pathway as an essential downstream factor of aforementioned EVs. Thus, our findings revealed a novel mechanism for the glioma-mediated TME establishment that may shed light on the development of therapeutic strategy for treating glioblastoma with higher efficacy.

Material And Methods

Animals and regents

C57BL/6J mice were purchased from Shanghai Laboratory Animal Center (Chinese Academy of Sciences) and were housed and maintained in the Comparative Medicine Facility of the Tongji University School of Medicine (Shanghai, China). All procedures were conducted in accordance with the protocols approved by the Institutional Animal Care and Use Committee at Tongji University School of Medicine.

Mouse NPCs (mNPCs) culture and treatment

Mouse cortical NPCs were isolated from gestational day E14 brain tissue as previously described [20]. Brain tissues were dissected and mechanically dissociated using forceps to remove the membranes and large blood vessels. Brain tissues were digested by Trypsin-EDTA (Life Technologies) and then plated on cell culture flasks in mouse NeuroCult NSC Proliferation Medium (StemCell Technologies, Vancouver, BC, Canada), supplemented with epidermal growth factor (EGF, 10 ng/ml, Novus Biologicals), basic fibroblast growth factor (bFGF, 20 ng/ml, Novus Biologicals) for selective neurosphere cultures and penicillin/streptomycin (1% v/v, Gibco). Neurospheres were passaged when they reached 100-150 μm in diameter.

U87 and A172 culture

The human glioblastoma cell lines U87 and A172 (American Type Culture Collection, Manassas, VA, USA) were authenticated by American Type Culture Collection using the short tandem repeat genotyping method. U87 and A172 cells were cultured in DMEM GlutaMax (Gibco) containing 10% FBS (Sigma-Aldrich) and penicillin/streptomycin (1% v/v) in humidified chamber (37 °C, 5% CO_2 incubator). U87 cells were passaged at 3-4 day intervals.

Isolation of EVs

The method for the isolation of extracellular vesicles has been described previously [21]. Briefly, 1×10^6 U87 or A172 cells were plated on 10 cm dish and grown to 70-80% confluence. Then, U87s or A172 were rinsed with PBS three times and incubated with serum-free DMEM GluMax for 24 hours. Media were harvested and first centrifuged at 300 × g for 10 minutes to remove free cells, at 3,000 × g for 20 minutes to remove cellular debris, and then at 10,000 × g for 30 minutes to remove intracellular organelles. Lastly, EVs were collected by ultracentrifugation at 100,000 × g for 2 hours. All centrifugation steps were performed at 4 °C.

Transmission electron microscopy (TEM)

EVs were fixed with paraformaldehyde, negatively stained, and then spread on the copper grids. The droplets of EVs were removed with filter paper and air-dried at room temperature. Images were obtained using transmission electron microscopy (JEM-1230, JEOL Ltd.).

Dynamic light scattering (DLS)

EVs were re-suspended in 100 μl PBS and then diluted as 1:10 in PBS. 500 μl sample were added into a microcuvette (ZEN0118, Malvern Instruments, UK) to measure size using Nano ZS90 (Malvern Instruments, UK) at 25 °C.

Nanoparticle tracking analysis (NTA)

The size and concentration of extracellular vesicles were measured with NanoSight NS300 system (Malvern Instruments, UK). Briefly, U87 and A172 cells were cultured in 10 cm culture dishes for 48 hours. Then, the medium was changed to serum-free medium for 24 hours. The supernatants were differentially centrifugated and resuspended with 100 µl PBS and diluted at 1:10 in PBS, and then 1 ml solution was used for NanoSight analysis.

EV uptake assay

For EVs tracking, EVs or PBS were fluorescently labeled with PKH26 Red Fluorescent Cell Linker Mini Kit (SigmaAldrich) according to manufacturer's protocol. The labeled EVs or PBS were added into mNPCs for 8 hours. Then, the samples were stained with F-Actin (Phalloidin) and DAPI and images were captured by Zeiss AX10 fluorescence microscope.

Western blot

EV pellets or cells were lysed in M-PER mammalian protein extraction reagent (Thermo Scientific) containing protease inhibitor (Thermo Scientific). Protein concentration was determined using the BCA (bicinchoninic acid) Protein Assay Kit (Pierce). An analytical 10% SDS polyacrylamide gel electrophoresis (SDS PAGE) was prepared and then transferred to polyvinyldifluoridene (PVDF) membranes (Millipore, Billerica, MA, USA). After blocking in 5% fat-free milk for 1 hour, the membrane was incubated with purified primary antibodies for phospho-PI3K (p-PI3K, 1:1,000; Cell Signaling Technologies), PI3K (1:1,000; Cell Signaling Technologies), phospho-Akt (Ser473) (p-Akt, 1:1,000; Cell Signaling Technologies), Akt (1:1,000; Cell Signaling Technologies), phospho-mTOR (p-mTOR, 1:1,000; Cell Signaling Technologies), mTOR (1:1,000; Cell Signaling Technologies), phospho-C-Raf (p-C-Raf, 1:1000; Cell Signaling Technologies), phospho-MEK1/2 (p-MEK1/2, 1:1,000; Cell Signaling Technologies), MEK1/2 (1:1,000; Cell Signaling Technologies), phospho-ERK1/2 (p-ERK1/2, 1:1,000; Cell Signaling Technologies), ERK1/2 (1:1,000; Cell Signaling Technologies), β-actin (Actin, 1:5,000; Proteintech), flotillin-1 (1:1,000; BDbiosciences), flotillin-2 (1:5,000; BDbiosciences), TSG101 (1:5,000; Abacm), Alix (1:2,000; Bioworld), Calreticulin (1:1,000; Abcam) overnight at 4 °C followed by a horseradish peroxidase-linked secondary anti-rabbit or anti-mouse antibody (1:5,000; Icllab). Antigen-antibody complexes were visualized by Pierce ECL Western Blotting Substrate (Thermo Scientific).

Immunocytochemistry

For immunofluorescence staining, mNPCs were plated on the coverslips and fixed using 4% paraformaldehyde (PFA) for 20 minutes, then permeabilized with 0.4% Triton-X in PBS for 15 minutes. Subsequently, the coverslips were blocked with1% BSA for 1 hour. mNPCs were incubated with primary

antibodies overnight including Nestin (1:500; Novus Biologicals) and Ki67 (1:1,000; Cell Signaling Technologies). Coverslips were washed with PBS three times and incubated for 1 hour at room temperature with secondary antibodies including anti-rabbit, mouse or chicken IgG (coupled with Alexa Fluor 488 or 568, Life Technologies). Nuclei were counter-stained with DAPI. Coverglasses were fixed on glass slides with Mounting Medium (Sigma-Aldrich). The images were captured by Zeiss AX10 fluorescence microscope. For quantification, the numbers of stained cells were quantified by Image-Pro Plus 6.0.

Transwell assay

8 mm pore size transwell system (Costar) were coated with diluted matrigel (1:80, matrigel:NPC basal medium) in humidified chamber (37 °C, 5% CO_2 incubator) for 30 minutes. Briefly, NPCs were dissociated into single cells and 2×10^5 cells/ml were resuspended in Mouse NeuroCult Proliferation Medium. The top chamber of the transwell was loaded with 100 µl of cell suspension containing either EVs or PBS. In the lower chamber, 600 µl of NPC proliferation medium was added. After 12 hours, the transwell inserts member was fixed with 4% PFA, and cells were removed by a cotton swab from the upper chamber. Migrated cells on the bottom of the membrane were stained with DAPI (Sigma Aldrich). For each insert, cells migrated through the pores were captured by Zeiss AX10 fluorescence microscope. Cell numbers were counted using Image-Pro Plus 6.0. The cell number of each insert-treated group was normalized to the cell number of the control group to analyze migration index.

Wound healing assay

mNPCs were seeded at 80% confluence in a 24-well plate coated with diluted matrigel. Each well was scratched using a 200 µl pipette tip. Each well was washed with PBS for three times and added NPC proliferation medium containing EVs or PBS. Images were captured at 0 hour and24 hours after the initial scratch. Images were captured by Olympus light microscopy.

EdU incorporation assay

Click-iT® EdU Imaging Kits (Thermo Scientific, #C10338) was used to analyze DNA synthesis according to the manufacturer's instructions. 2.5×10^5 mNPCs cell were planted on 35 mm Coverglass-Bottom Dish (Cellvis, #D35-14-1-N). After 24 hours, medium was changed with fresh medium containing 50 µg/ml EVs or PBS for 24 hours. EdU was added to medium before 2 hours of fixation. Then, cells were fixed using 4% PFA for 20 minutes, and permeabilized with 0.5% triton-X100 in PBS for 15 minutes. Click-iT® reaction cocktails (Thermo Scientific) was added to dish for reacting for 30 minutes at room temperature and protected from light. Subsequently, cell nuclei were stained with DAPI. For each dish, 6 fields were randomly taken using Zeiss AX10 fluorescence microscope. The numbers of EdU-labled and DAPI-stained cells were counted by Image-Pro Plus 6.0.

Cell proliferation assay

Briefly, 15 μg/ml glioblastoma-derived EVs were co-cultured with 5000 cells/well mNPCs on 96-well plates for 24 hours, then changed with NPC proliferation medium without EVs and cultured for 48 hours. Cell viability was measured by CCK-8 (Yeasen, #40203ES80) assays at different time points. Experiments were handled according to the manufacturer's instructions. Absorbance was measured at 570 nm and 450 nm and analyzed using SpectraMax M5 microplate readers (Molecular Devices).

Protein identification and bioinformatics analysis

The resulting MS/MS data were processed using Maxquant search engine (v.1.5.2.8). Tandem mass spectra were searched against uniprot database concatenated with reverse decoy database. Trypsin/P was specified as cleavage enzyme allowing up to 4 missing cleavages. FDR was adjusted to < 1% and minimum score for modified peptides was set > 40. Proteins were classified by GO annotation into three categories: biological process, cellular compartment and molecular function. For each category, a two-tailed Fisher's exact test was employed to test the enrichment of the differentially expressed protein against all identified proteins. The GO with a corrected *p*-value < 0.05 is considered significant. Encyclopedia of Genes and Genomes (KEGG) database was used to identify enriched pathways by a two-tailed Fisher's exact test to test the enrichment of the differentially expressed protein against all identified proteins. The pathway with a corrected *p*-value < 0.05 was considered significant.

Statistical analyses

All results are the means of at least three independent experiments ± SD. Data from two groups were evaluated statistically by two-tailed, paired or unpaired student *t* test. **p*<0.05, ***p*<0.01, ****p*<0.001 and *****p*<0.0001, in comparison to control.

Results

Characterization of EVs released from U87 and A172 cells

We firstly characterized U87-derived EVs (U87-EVs) and A172-derived ones (A172-EVs). EVs were collected using differential centrifugation from the serum-free culture media of U87 and A172 cells. Negatively stained TEM was used to observe the morphology of EVs. The resuspended U87-EVs (Fig. 1A) and A172-EVs (Fig.1D) showed typical cup-shaped EV morphology under negative staining in TEM, confirming that those vesicles released from U87 or A172 cells were indeed EVs. Subsequently, DLS and NTA were utilized to analyze the size of EVs. Both DLS and NTA analyses demonstrated similar sizes for EVs released from U87 (Fig. 1B, C) and A172 (Fig. 1E, F), suggesting there was no significant difference in size distributions of different types of EVs. The sizes of EVs revealed by DLS analysis (~200 um) were larger than that of EVs revealed by NTA analysis (~120 nm), which was probably due to the physiological

feature of DLS that favors the detection of larger particles over small particles. We then applied cells lysis, U87-EVs, and A172-EVs, to western blot to confirm the expression of specific EVs markers Alix (ALG-2 interacting protein), Flotillin-1, Flotllin-2, and TSG101 (Fig. 1G, H). The absence of Calreticulin (a marker for endoplasmic reticulum) in EVs indicates the purification of EVs without contamination of cell debris and organelles. To test the uptake of EVs, we co-cultured PKH-26 labeled U87-EVs and A172-EVs with mNPCs. PKH-26 fluoresence was observed in mNPCs after 8 hours' co-culture (Fig. 1I, J), which, indicated EVs were biologically active and could be taken up by mNPCs.

EVs released from glioblastoma facilitate mNPCs proliferation

Increasing evidences have shown abnormal proliferation of NPCs in glioblastoma microenvironment [21, 22]. We hypothesized that glioblastoma-derived EVs trigger NPCs' proliferation in the patients with recurrent glioblastoma. To verify this premise, we examined the proliferation of mNPCs treated with either U87-EVs or A172-EVs with an EdU assay. U87-EVs-treated mNPCs had higher proportions of EdU positive cells (32.8% ± 1.141%) than control mNPCs (26.23% ± 1.069%) (Fig. 2A). Similarly, A172-EVs-treated mNPCs had higher proportion of EdU positive cells (52.16% ± 2.87%) than control mNPCs (40.43% ± 1.36%) (Fig. 2B). Apart from that, our results showed that U87-EVs-treated mNPCs had significantly higher proportion of Ki67-positive cells (78.13% ± 2.958%) as compared with control mNPCs (54.77% ± 3.565%) (Fig. 2C). Similarly, A172-EVs-treated mNPCs had larger proportion of Ki67 positive cells (76.51% ± 1.961%) as compared with control mNPCs (65.06% ± 1.779%) (Fig. 2E). Additionally, CCK-8 assay exhibited similar effect as it showed that U87-EVs or A172-EVs promoted the proliferation of mNPCs after co-culturing mNPCs with EVs for 48-72 hours (Fig. 2D, F). These data indicated that glioblastoma-derived EVs facilitate mNPCs' proliferation.

Glioblastoma-derived EVs enhance mNPCs migration

Previous reports indicated that NPCs had a tropism for glioblastoma as NPCs implanted at distant sites away from the site of glioma migrated to the tumor across normal tissues [11, 12]. We utilized transwell assay and wound healing assay to investigate whether the EVs released from glioblastoma enhanced NPCs migration. In transwell assay, we found that the migration index of mNPCs was significantly enhanced by U87-EVs (migrated cell numbers, 174.5 ± 6.661) compared with control groups (migrated cell numbers, 133.8 ± 4.581) (Fig. 3A). Similarly, the migration index of mNPCs was significantly increased by A172-EVs (migrated cell numbers, 150.8 ± 9.165) compared with control mNPCs (migrated cell numbers, 95.82±9.34) (Fig. 3B). In wound healing assay, our data showe that U87-EVs significantly promoted migratory capacity of mNPCs (42.62% ± 1.447%) compared with PBS controls (23.94% ± 2.06%) (Fig. 3C). Likely, A172-EVs enhanced the migratory capacity of mNPCs (39.72% ± 2.578%) compared with control mNPCs (21.07% ± 1.159%) (Fig. 3D). These results indicated that glioblastoma-derived EVs facilitated mNPCs to show a tropism for glioblastoma.

Glioblastoma-derived EVs altered cell signaling of mNPCs

To determine the molecular contents that may be responsible for increased proliferation and migration of glioblastoma-EVs-treated mNPCs, we performed proteomic profiling of U87-EVs-treated mNPCs (Supplementary Fig. 1). Since both U87-EVs and A172-EVs exhibited similar influences on mNPCs' regulation, we only used U87-EVs for following mechanism identification and confirmation studies. Proteomic analysis identified 187 upregulated and 141 downregulated proteins in U87-EVs-treated mNPCs versus control mNPCs (Fig. 4A). These differentially expressed proteins were majorly located in cytoplasm (31.91%), nucleus (27.66%), and mitochandria (13.07%) (Fig. 4B). Gene Ontology analysis revealed that the upregulated proteins were mainly involved in cancer-related biological processes in U87-EVs-treated mNPCs, such as positive regulation of cell cycle arrest, mRNA catabolic process, and positive regulation of cell proliferation, while the downregulated proteins were associated with RNA processing, transcription, and translation (Fig. 4C, D). KEGG analysis confirmed that the upregulated proteins in mNPCs treated by U87-EVs were strongly linked with cancer-related signaling pathways, such as Thyroid hormone signaling, AMPK signaling, and metabolic pathways (Fig. 4E). In contrast, the downregulated proteins were involved in pathways that induce cell stress and neurodegeneration including Huntington's disease, Parkinson's disease, and Oxidative phosphorylation (Fig. 4F).

Among the altered cell signaling pathways in U87-EVs-treated mNPCs (Fig. 4E), both thyroid hormone signaling pathway and AMPK signaling pathway are mediated by downstream PI3K-Akt signaling pathway. Interestingly, by analyzing the proteome data from published article from Haraszti et. al. [22], we confirmed that proteins participating in PI3K-Akt pathway were significantly enriched in U87-EVs (Supplementary Fig. 2) and specifically sorted into U87-EVs (Supplementary Fig. 3). To verify the results obtained from proteomic analyses, we next performed western blot to examine the activities of PI3K-Akt pathway in U87-EVs-treated mNPCs (Fig. 4G). Indeed, we observed upregulation of PI3K-Akt signaling pathway molecules, including phosphorylated PI3K, PDK1, Akt, and mTOR, post glioblastoma-derived EV treatment in an approximately time-dependent manner, indicating the induction of PI3K-Akt-mTOR signaling in mNPCs by U87-EVs.

Glioblastoma-derived EVs increased the proliferation and migration of mNPCs through upregulating PI3K-Akt signaling

To verify whether the elevated activities of PI3K-Akt signaling is responsible for enhanced mNPCs proliferation and migration after being treated by U87-EVs, we used a PI3K inhibitor, Wortmannin, to block PI3K-Akt signaling in U87-EVs-treated mNPCs. As expected, Wortmannin treatment significantly inhibited the phosphorylation of PI3K, PDK1, Akt, and mTOR (Fig. 5). Importantly, both EdU incorporation assay (Fig. 6A) and Ki67 immunocytochemistry (Fig. 6B) revealed that the suppression of PI3K-Akt pathway by Wortmannin reversed the enhanced proliferation of U87-EVs-treated mNPCs. Likewise, both transwell (Fig.

7A) and wound healing assay (Fig. 7B) showed that Wortmannin treatment significantly lowered the increased migration capacities of U87-EVs-treated mNPCs. These results showed that inhibiting PI3K-Akt pathway were able to abrogate the positive effects of glioblastoma-derived EVs on proliferation and migration of mNPCs, indicating the activation of PI3K-Akt pathway as a key intracellular mechanisms in the phenotype transtion of mNPCs that induced by TME.

Discussion

Glioblastoma is known to affect almost all types of cells in the tumor environ and recruit nonneoplastic cells to support tumor growth, subsistence, and encroachment into nontumor regions [8]. Glioblastomas stimulate angiogenesis and consolidate existing vasculature by secreting regulatory growth factors like vascular endothelial growth factor (VEGF) or hepatoma-derived growth factor (HDGF) [23, 24]. Glioblastoma suppress both innate and adaptive immune cell functions: microglia are disarmed and lose their abilities to recognize foreign/toxic elements [25]; T cells are suppressed with a complex array of immune regulatory mechanisms to allow neoplastic cells escape the immune checkpoints [8, 26–28]. Peritumoral astrocytes' transcriptome and secretome are altered by glioma resection to promote cellular proliferation and migration [9]. More importantly, glioblastoma cells induce NPCs to migrate toward the site of tumor [11] and exhibit transformed phenotypes [29]. In our study, we confirmed the positive effects of glioblastoma cells on proliferation and migration of NPCs, clearly presenting the influence of TME on normal cells.

Cellular communication between tumor cells and surrounding cells plays a key role in this glioblastoma "hijacking" of the brain. Soluble factors secreted by tumor cells, like transforming growth factor- β (TGFβ), IL-6, Notch, platelet-derived growth factor (PDGF), epidermal growth factor (EGF), VEGF, and stromal cell-derived factor 1 (SDF1; also known as CXCL12), serve as important signaling molecules as they bind to receptors located on target cells [11]. Apart from soluble factors, tumor cells utilize other forms of communication to transfer non-secreted factors like genetic materials, transcription factors, and even organelles like mitochondria or nuclei via gap junctions, EVs, or nanotubes [8, 30, 31]. These different routes of interactions between tumor cells and nonneoplastic cells in the TME facilitate glioblastoma to create a flexible environment that adapts to challenges like resection, chemo-, or radiotherapy, thus survive and grow. Among aforementioned factors, EVs have emerged as a key communicator between glioblastoma and normal cells. EVs have important functions: EVs contain both soluble and non-soluble contents and transfer them from donor cells to recipient cells. In glioblastoma, EVs derived from donor tumor cells transfer soluble factors like cytokines and chemokines, as well as non-soluble molecules like transcription factors, RNA, DNA, lipids, and metabolites, to target normal cells and subsequently change their phenotypes [32]. Contents packaged in EVs are usually stable and free from enzyme digestion [33], enabling effective steady distant cellular communication. In this study, we show that EVs mediate the influences of glioblastoma on proliferation and migration of NPCs. Our study provides new evidences for the intercellular communication between glioblastoma cells and NPCs, which further substantiates the components of TME and extends the interaction network of these components.

EVs achieve their function via delivering bioactive cargos into recipient cells, which can influence various intracellular signaling pathways. In our study, we identified that PI3K-Akt pathway as the key one that mediates the positive effects of EVs on proliferation and migration of mNPCs. PI3K-Akt signaling pathway is well-known one being upregulated in cancer cells that regulates diverse cellular functions including survival, proliferation, migration, and metabolism [34, 35]. More than 60% of glioblastoma cases have been linked with at least one mutated or dysregulated PI3K-Akt-mTOR pathway proteins [36–38]. Mutations of *PIK3CA*, the gene encoding the p110α subunit of PI3K, or mutations of *PIK3R1*, the gene encoding the p85 regulatory subunit of PI3K, have been demonstrated in approximately 15% of patients with glioblastoma [38–40]. Loss of function, chromosomal abnormalities, or epigenetic gene silencing of PTEN, the negative regulator of PI3K-Akt pathway, have been found in approximately 40% of glioblastoma cases and have been linked with poor prognosis [41]. PI3K-Akt signaling partly regulates hypoxia-inducible-factor (HIF) stabilization, which promotes glioblastoma division [42]. The PI3K-Akt pathway-induced HIF activation also modulates Warburg effect, the most widely-accepted metabolic shift that cancer cells heavily depend on for additional energy supply [34, 43]. More importantly, activation of PI3K-Akt pathway components in mNPCs directly induced glioblastoma formation *in vivo*, suggesting the direct link of PI3K-Akt pathway to glioblastoma-induced NPC phenotype change [44]. Furthermore, studies show that activation of PI3K-Akt-mTOR enhanced tumor cell tolerance to chemotherapy [45]. To date, to overcome the commonly occurred radio- or chemo-resistance, immunotherapy is introduced in combination with surgery, chemo, and radiotherapy in glioma treatment. Multiple strategies of glioblastoma immunotherapy are via PI3K-Akt signaling inhibition [46, 47]. These therapies prove effective in animal models, however, almost fail to make any difference in clinic given the high heterogeneity of cellular and molecular components in glioblastoma [8, 48]. Blocking EVs release from glioma tumor cells might be a promising strategy to inhibit the activation of PI3K-Akt pathway from the source in combination with other forms of therapy, which, needs to be further studied in future research.

Interestingly, our results did reveal that components of ERK pathway were also significantly upregulated in a time-dependent manner (**Supplementary Fig. 4**), demonstrating heightened expressions of cancerous shift-related signaling molecules other than PI3K-Akt pathway components in U87 EVs-treated mNPCs. ERK pathway is strongly associated with poor prognosis and glioblastoma patient survival [49]. In glioblastoma, ERK pathway has been reported to promote angiogenesis once activated by VEGF under hypoxia [49], to enhance drug resistance [50], and maintain high glutamine metabolism [51]. Similar to PI3K-Akt pathway, ERK signaling has also been considered as a therapeutic target of glioblastoma. Ethyl pyruvate [52], trametinib [53], amentoflavone [54], hyperforin [55], berberine [56], imipramine [57], and protein neddylation inhibitor MLN4924 [58] inhibit glioblastoma cells migration and invasion via suppressing ERK pathway. Among them, several drugs has been applied in clinical trials such as trametinib (ClinicalTrials.gov Identifier: NCT03363217) [53]. In our study, the treatment of Wortmannin also significantly inhibited the activation of ERK pathway that is induced by U87-EVs (**Supplementary Fig. 5**), suggesting that ERK pathway may act as a downstream factor of PI3K-Akt pathway and both pathways may work together in mediating the tumorigenic effects of glioblastoma-derived EVs.

Given the fact that glioblastoma-derived EVs significantly promote proliferation and migration of mNPCs, there comes an important question that whether or not U87-EVs confer a glioma stem cell (GSC)-like phenotype to mNPCs [59]. Presenting stem cell properties like self-renewal and multi-lineage differentiation potentials, GSCs are resistant to radiotherapy and have the potential to induce angiogenesis, metastasis and modulate therapeutic responses [60]. Compared with non-stem tumor cells, GSCs present a heightened DNA repair capacity and recover rapidly from conventional therapeutic stress [59, 61]. However so far, due to that a subpopulation of GSCs shares the same set of biomarkers with normal NPCs [62, 63], there remains in lack of direct evidence to precisely define the transition of mNPCs to GSCs. Therefore, it is difficult to prove that glioblastoma-derived EVs alter normal NPCs to acquire GSC phenotype, although our results indicate significant upregulation of cancer metabolic signaling molecules in EV-treated mNPCs and that these mNPCs present elevated proliferation and migration capacity. With more comprehensive investigations, new approaches and indexes can be developed to distinguish GSCs from NPCs and the effects of glioblastoma-derived EVs on mNPC phenotype transition can be further validated.

Conclusions

Taken together, our study demonstrated glioblastoma-derived EVs promoted proliferation and migration of mNPCs,suggesting the alteration of mNPCs' phenotype via glioblastoma-derived EVs treatment. Furthermore, we identified key downstream factor of glioblastoma-derived EVs, PI3K-Akt pathway, as elevated proliferation and migration of mNPCs post EVs treatment could be reversed by inhibiting PI3K-Akt signaling pathway. These findings expanded our current knowledge of tumor-nontumor interactions in the glioblastoma microenvironment and provided a new direction to overcome the current challenges (such as frequent recurrence) of glioblastoma treatment.

List Of Abbreviations

DLS: Dynamic light scattering

EGF: Epidermal growth factor

EVs: Extracellular vesicles

GSCs: Glioma stem cells

HDGF: Hepatoma-derived growth factor

mNPCs: Mouse neural progenitor cells

NPCs: Neural progenitor cells

NTA: Nanoparticle trafficking

PDGF: Platelet-derived growth factor

PFA: Paraformaldehyde

TEM: Transmission electron microscopy

TME: Tumor microenvironment

TGFβ: Transforming growth factor- β

VEGF: Vascular endothelial growth factor

Declarations

Acknowledgements

We thank Dr. Chao Lin (Tongji University, Shanghai, China) for the assistance with the DLS.

Funding

This work was supported in part by research grants from the Major Research plan of the National Natural Science Foundation of China (No. 91949204 to JCZ), the State Key Program of the National Natural Science Foundation of China (No. 81830037 to JCZ), the National Institutes of Health (1R01NS097195-01 to JCZ), the National Natural Science Foundation of China (No. 81901333 to XX), Shanghai Sailing Program (No. 19YF1451700 to XX), National Natural Science Foundation of China (No. 81801063 to YW), and Shanghai Municipal Health Commission (No.20204Y0031 to YW).

Availability of data and materials

The datasets generated for this study are available on reasonable request to the corresponding authors.

Authors' contributions

JCZ YH XX LY JP designed the experiments. JP SS YM LQ ZF XX performed the experiments and analyzed the data. JP YL YW XX prepared the manuscript. All authors read and approved the final manuscript.

Competing interests

The authors declare that they have no competing interests.

Consent for publication

Not applicable.

Ethics Statement

N/A.

References

1. Louis, D.N., et al., *The 2016 World Health Organization Classification of Tumors of the Central Nervous System: a summary.* Acta Neuropathol, 2016. **131**(6): p. 803-20.
2. Hardee, M.E. and D. Zagzag, *Mechanisms of glioma-associated neovascularization.* Am J Pathol, 2012. **181**(4): p. 1126-41.
3. Stupp, R., et al., *Effects of radiotherapy with concomitant and adjuvant temozolomide versus radiotherapy alone on survival in glioblastoma in a randomised phase III study: 5-year analysis of the EORTC-NCIC trial.* Lancet Oncol, 2009. **10**(5): p. 459-66.
4. Quail, D.F. and J.A. Joyce, *The Microenvironmental Landscape of Brain Tumors.* Cancer Cell, 2017. **31**(3): p. 326-341.
5. Wang, Q., et al., *Tumor Evolution of Glioma-Intrinsic Gene Expression Subtypes Associates with Immunological Changes in the Microenvironment.* Cancer Cell, 2017. **32**(1): p. 42-56 e6.
6. Audia, A., et al., *The Impact of the Tumor Microenvironment on the Properties of Glioma Stem-Like Cells.* Front Oncol, 2017. **7**: p. 143.
7. Batlle, E. and H. Clevers, *Cancer stem cells revisited.* Nat Med, 2017. **23**(10): p. 1124-1134.
8. Broekman, M.L., et al., *Multidimensional communication in the microenvirons of glioblastoma.* Nat Rev Neurol, 2018. **14**(8): p. 482-495.
9. Okolie, O., et al., *Reactive astrocytes potentiate tumor aggressiveness in a murine glioma resection and recurrence model.* Neuro Oncol, 2016. **18**(12): p. 1622-1633.
10. Takano, T., et al., *Glutamate release promotes growth of malignant gliomas.* Nat Med, 2001. **7**(9): p. 1010-5.
11. Heese, O., et al., *Neural stem cell migration toward gliomas in vitro.* Neuro Oncol, 2005. **7**(4): p. 476-84.
12. Aboody, K.S., et al., *Neural stem cells display extensive tropism for pathology in adult brain: evidence from intracranial gliomas.* Proc Natl Acad Sci U S A, 2000. **97**(23): p. 12846-51.
13. Tkach, M. and C. Thery, *Communication by Extracellular Vesicles: Where We Are and Where We Need to Go.* Cell, 2016. **164**(6): p. 1226-1232.
14. Maas, S.L.N., X.O. Breakefield, and A.M. Weaver, *Extracellular Vesicles: Unique Intercellular Delivery Vehicles.* Trends Cell Biol, 2017. **27**(3): p. 172-188.

15. Minciacchi, V.R., et al., *Large oncosomes contain distinct protein cargo and represent a separate functional class of tumor-derived extracellular vesicles.* Oncotarget, 2015. **6**(13): p. 11327-41.
16. Lai, C.P., et al., *Dynamic biodistribution of extracellular vesicles in vivo using a multimodal imaging reporter.* ACS Nano, 2014. **8**(1): p. 483-494.
17. Wu, B., et al., *Glutaminase-containing microvesicles from HIV-1-infected macrophages and immune-activated microglia induce neurotoxicity.* Mol Neurodegener, 2015. **10**: p. 61.
18. Ma, Y., et al., *Exosomes released from neural progenitor cells and induced neural progenitor cells regulate neurogenesis through miR-21a.* Cell Commun Signal, 2019. **17**(1): p. 96.
19. Mbengue, A., et al., *A molecular mechanism of artemisinin resistance in Plasmodium falciparum malaria.* Nature, 2015. **520**(7549): p. 683-7.
20. Tian, C., et al., *Direct conversion of dermal fibroblasts into neural progenitor cells by a novel cocktail of defined factors.* Curr Mol Med, 2012. **12**(2): p. 126-37.
21. Wang, K., et al., *TNF-alpha promotes extracellular vesicle release in mouse astrocytes through glutaminase.* J Neuroinflammation, 2017. **14**(1): p. 87.
22. Haraszti, R.A., et al., *High-resolution proteomic and lipidomic analysis of exosomes and microvesicles from different cell sources.* J Extracell Vesicles, 2016. **5**: p. 32570.
23. Jhaveri, N., T.C. Chen, and F.M. Hofman, *Tumor vasculature and glioma stem cells: Contributions to glioma progression.* Cancer Lett, 2016. **380**(2): p. 545-51.
24. Jain, R.K., et al., *Angiogenesis in brain tumours.* Nat Rev Neurosci, 2007. **8**(8): p. 610-22.
25. Roesch, S., et al., *When Immune Cells Turn Bad-Tumor-Associated Microglia/Macrophages in Glioma.* Int J Mol Sci, 2018. **19**(2).
26. Martinez, G.J., et al., *The transcription factor NFAT promotes exhaustion of activated CD8(+) T cells.* Immunity, 2015. **42**(2): p. 265-278.
27. Park, B.V., et al., *TGFbeta1-Mediated SMAD3 Enhances PD-1 Expression on Antigen-Specific T Cells in Cancer.* Cancer Discov, 2016. **6**(12): p. 1366-1381.
28. Voron, T., et al., *VEGF-A modulates expression of inhibitory checkpoints on CD8+ T cells in tumors.* J Exp Med, 2015. **212**(2): p. 139-48.
29. Wang, J., et al., *Glioblastoma extracellular vesicles induce the tumour-promoting transformation of neural stem cells.* Cancer Lett, 2019. **466**: p. 1-12.
30. Wang, X., et al., *Animal cells connected by nanotubes can be electrically coupled through interposed gap-junction channels.* Proc Natl Acad Sci U S A, 2010. **107**(40): p. 17194-9.
31. Osswald, M., et al., *Brain tumour cells interconnect to a functional and resistant network.* Nature, 2015. **528**(7580): p. 93-8.
32. D'Asti, E., et al., *Extracellular Vesicles in Brain Tumor Progression.* Cell Mol Neurobiol, 2016. **36**(3): p. 383-407.
33. Xia, X., et al., *Exosomal miRNAs in central nervous system diseases: biomarkers, pathological mediators, protective factors and therapeutic agents.* Prog Neurobiol, 2019. **183**: p. 101694.

34. Thomas, T.M. and J.S. Yu, *Metabolic regulation of glioma stem-like cells in the tumor micro-environment.* Cancer Lett, 2017. **408**: p. 174-181.
35. Mellinghoff, I.K., et al., *Molecular determinants of the response of glioblastomas to EGFR kinase inhibitors.* N Engl J Med, 2005. **353**(19): p. 2012-24.
36. Cancer Genome Atlas Research, N., *Comprehensive genomic characterization defines human glioblastoma genes and core pathways.* Nature, 2008. **455**(7216): p. 1061-8.
37. Masica, D.L. and R. Karchin, *Correlation of somatic mutation and expression identifies genes important in human glioblastoma progression and survival.* Cancer Res, 2011. **71**(13): p. 4550-61.
38. Kita, D., et al., *PIK3CA alterations in primary (de novo) and secondary glioblastomas.* Acta Neuropathol, 2007. **113**(3): p. 295-302.
39. Gallia, G.L., et al., *PIK3CA gene mutations in pediatric and adult glioblastoma multiforme.* Mol Cancer Res, 2006. **4**(10): p. 709-14.
40. Broderick, D.K., et al., *Mutations of PIK3CA in anaplastic oligodendrogliomas, high-grade astrocytomas, and medulloblastomas.* Cancer Res, 2004. **64**(15): p. 5048-50.
41. Koul, D., *PTEN signaling pathways in glioblastoma.* Cancer Biol Ther, 2008. **7**(9): p. 1321-5.
42. Soeda, A., et al., *Hypoxia promotes expansion of the CD133-positive glioma stem cells through activation of HIF-1alpha.* Oncogene, 2009. **28**(45): p. 3949-59.
43. Mauer, J., J.L. Denson, and J.C. Bruning, *Versatile functions for IL-6 in metabolism and cancer.* Trends Immunol, 2015. **36**(2): p. 92-101.
44. Holland, E.C., et al., *Combined activation of Ras and Akt in neural progenitors induces glioblastoma formation in mice.* Nat Genet, 2000. **25**(1): p. 55-7.
45. Wen, P.Y., et al., *Current clinical development of PI3K pathway inhibitors in glioblastoma.* Neuro Oncol, 2012. **14**(7): p. 819-29.
46. Venkatesh, H.S., et al., *Targeting neuronal activity-regulated neuroligin-3 dependency in high-grade glioma.* Nature, 2017. **549**(7673): p. 533-537.
47. Xi, X., et al., *ACT001, a novel PAI-1 inhibitor, exerts synergistic effects in combination with cisplatin by inhibiting PI3K/AKT pathway in glioma.* Cell Death Dis, 2019. **10**(10): p. 757.
48. Sanai, N., A. Alvarez-Buylla, and M.S. Berger, *Neural stem cells and the origin of gliomas.* N Engl J Med, 2005. **353**(8): p. 811-22.
49. Jiang, Y., et al., *Overexpression of Limb-Bud and Heart (LBH) promotes angiogenesis in human glioma via VEGFA-mediated ERK signalling under hypoxia.* EBioMedicine, 2019. **48**: p. 36-48.
50. Berberich, A., et al., *cMyc and ERK activity are associated with resistance to ALK inhibitory treatment in glioblastoma.* J Neurooncol, 2020. **146**(1): p. 9-23.
51. Yang, R., et al., *EGFR activates GDH1 transcription to promote glutamine metabolism through MEK/ERK/ELK1 pathway in glioblastoma.* Oncogene, 2020. **39**(14): p. 2975-2986.
52. Huang, Q., et al., *Ethyl pyruvate inhibits glioblastoma cells migration and invasion through modulation of NF-kappaB and ERK-mediated EMT.* PeerJ, 2020. **8**: p. e9559.

53. Perreault, S., et al., *A phase 2 study of trametinib for patients with pediatric glioma or plexiform neurofibroma with refractory tumor and activation of the MAPK/ERK pathway: TRAM-01.* BMC Cancer, 2019. **19**(1): p. 1250.
54. Hsu, F.T., et al., *Amentoflavone Effectively Blocked the Tumor Progression of Glioblastoma via Suppression of ERK/NF- kappa B Signaling Pathway.* Am J Chin Med, 2019. **47**(4): p. 913-931.
55. Hsu, F.T., et al., *Hyperforin induces apoptosis through extrinsic/intrinsic pathways and inhibits EGFR/ERK/NF-kappaB-mediated anti-apoptotic potential in glioblastoma.* Environ Toxicol, 2020. **35**(10): p. 1058-1069.
56. Jin, F., et al., *Berberine inhibits angiogenesis in glioblastoma xenografts by targeting the VEGFR2/ERK pathway.* Pharm Biol, 2018. **56**(1): p. 665-671.
57. Hsu, F.T., I.T. Chiang, and W.S. Wang, *Induction of apoptosis through extrinsic/intrinsic pathways and suppression of ERK/NF-kappaB signalling participate in anti-glioblastoma of imipramine.* J Cell Mol Med, 2020. **24**(7): p. 3982-4000.
58. Han, S., et al., *The Protein Neddylation Inhibitor MLN4924 Suppresses Patient-Derived Glioblastoma Cells via Inhibition of ERK and AKT Signaling.* Cancers (Basel), 2019. **11**(12).
59. Bao, S., et al., *Glioma stem cells promote radioresistance by preferential activation of the DNA damage response.* Nature, 2006. **444**(7120): p. 756-60.
60. Ma, Q., et al., *Cancer Stem Cells and Immunosuppressive Microenvironment in Glioma.* Front Immunol, 2018. **9**: p. 2924.
61. Huang, Z., et al., *Cancer stem cells in glioblastoma–molecular signaling and therapeutic targeting.* Protein Cell, 2010. **1**(7): p. 638-55.
62. Singh, S.K., et al., *Identification of human brain tumour initiating cells.* Nature, 2004. **432**(7015): p. 396-401.
63. Beier, D., et al., *CD133(+) and CD133(-) glioblastoma-derived cancer stem cells show differential growth characteristics and molecular profiles.* Cancer Res, 2007. **67**(9): p. 4010-5.

Figures

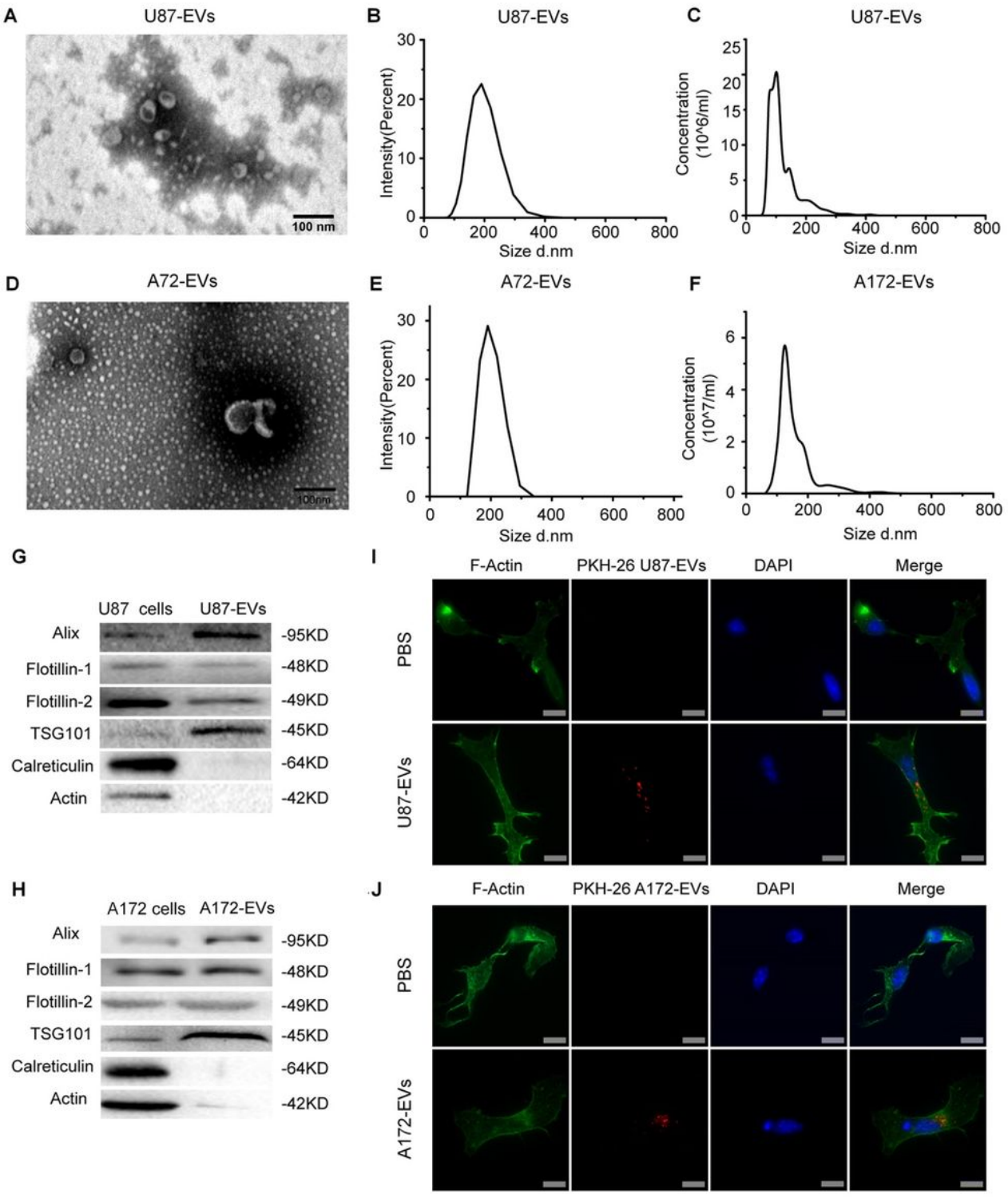

Figure 1

Characterization of EVs derived from U87 and A172 cells. A. TEM characterization of the morphology of U87-EVs. B. DLS characterization of the size and concentration of U87-EVs. C. NTA characterization of the size and concentration of U87-EVs. D. TEM characterization of the morphology of A172-EVs. E. DLS characterization of the size and concentration of A172-EVs. F. NTA characterization of the size and concentration of A172-EVs. G. Western blot characterization of expressions of EVs markers of U87-EVs.

H. Western blot characterization of expressions of EVs markers of A172-EVs. I. Immunofluorescence characterization of the activity of U87-EVs. J. Immunofluorescence characterization of the activity of A172-EVs. Scale bar, 100 nm (A, B) and 10 μm (I, J).

Fig.2

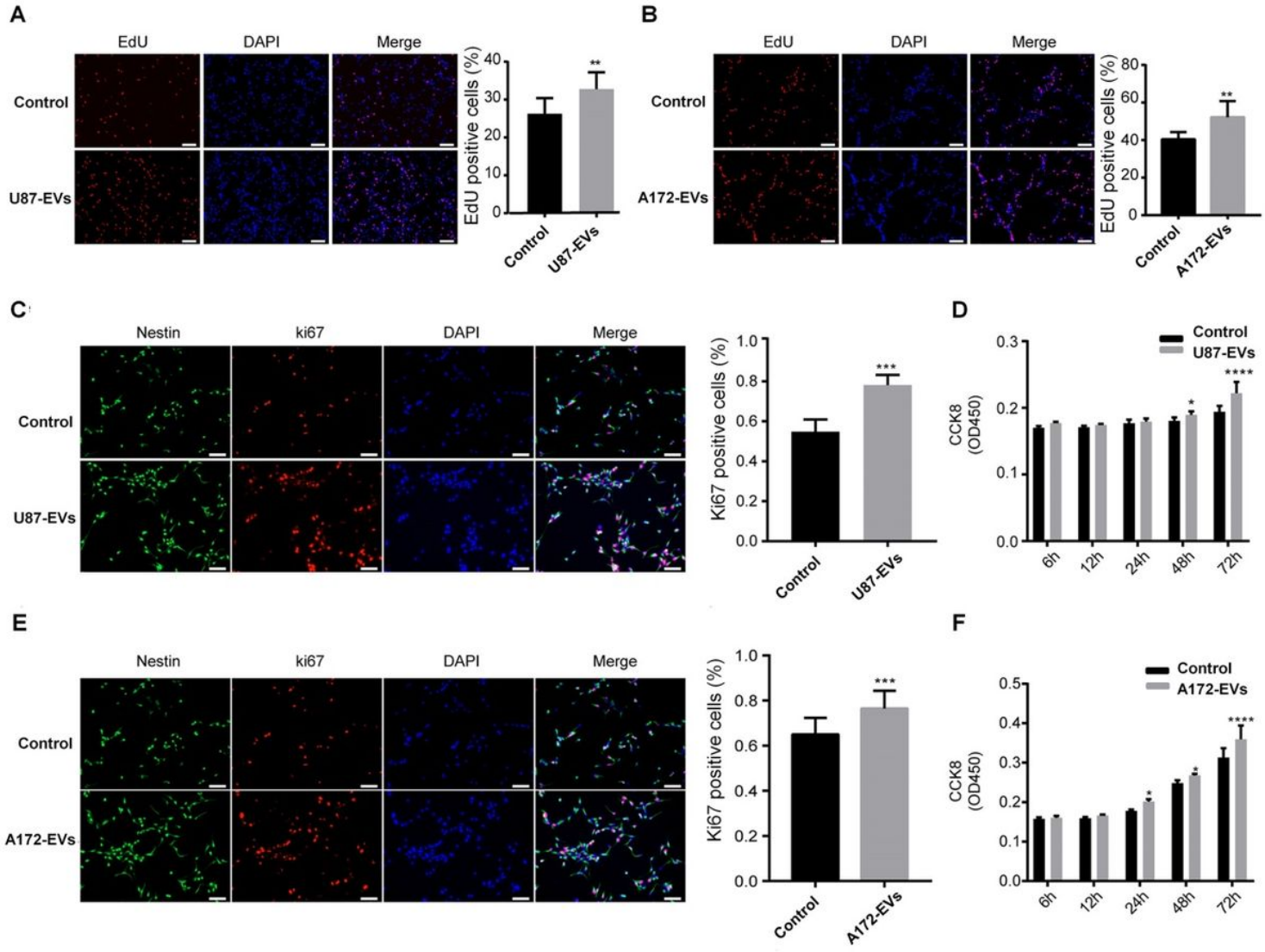

Figure 2

Glioblastoma-derived EVs promote the proliferation of mNPCs. A. U87-EVs-treated mNPCs exhibited higher proportion of EdU positive cells than control cells in the EdU incorporation assay. B. A172-EVs-treated mNPCs exhibited higher proportion of EdU positive cells than control cells in the EdU incorporation assay. C. U87-EVs-treated mNPCs exhibited significantly higher proportion of Ki67 positive cells than control cells. D. U87-EVs-treated mNPCs exhibited significantly higher CCK8 signal than control cells in a time-dependent manner. E. A172-EVs-treated mNPCs exhibited significantly higher proportion of Ki67 positive cells than control cells. F. A172-EVs-treated mNPCs exhibited significantly higher CCK8 signal than control cells in a time-dependent manner. Results are presented as the mean ± SD of three independent experiments. **p<0.01, ***p<0.001 and ****p<0.0001, in comparison with control. Scale bar, 100 μm (A, B) and 200 μm (C, E).

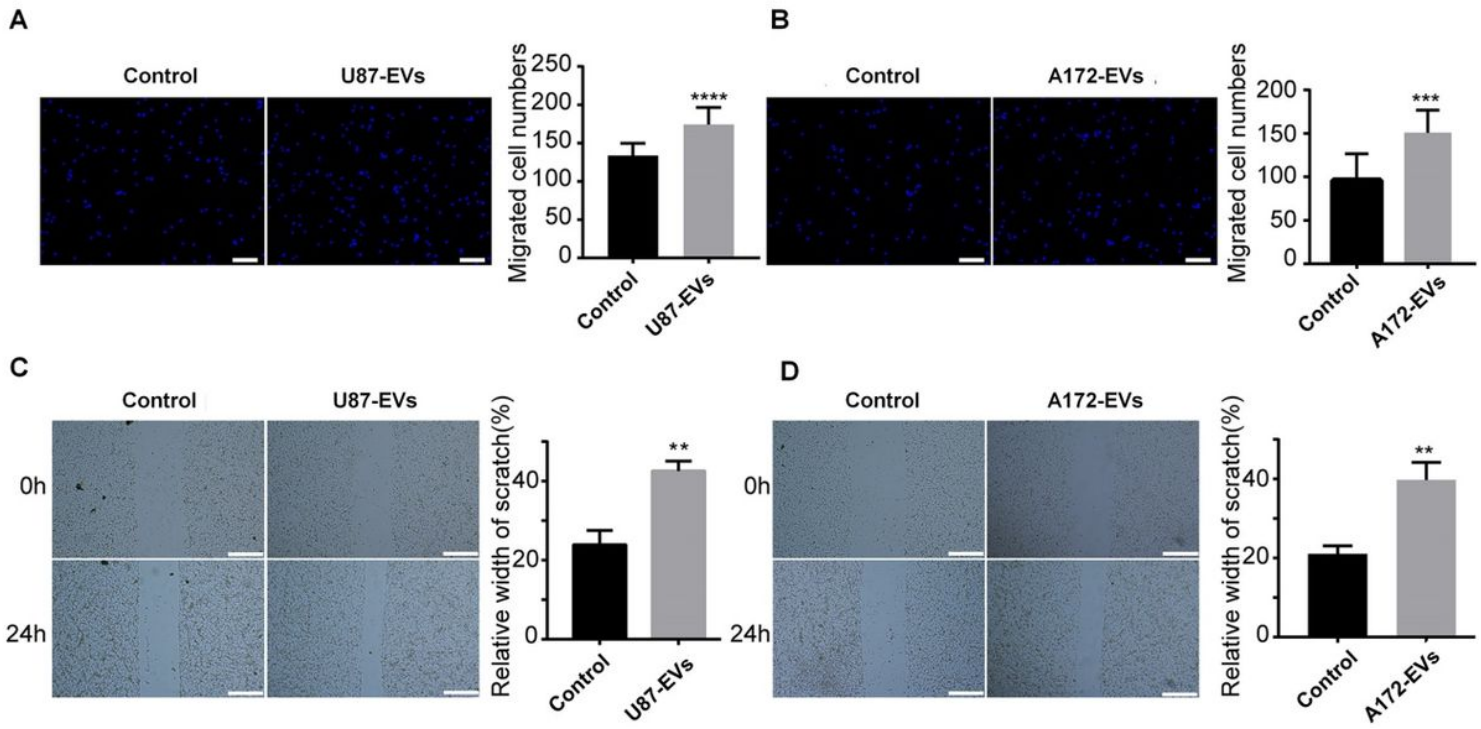

Figure 3

Glioblastoma-derived EVs elevate the migration of mNPCs. A. U87-EVs-treated mNPCs had significantly more migrated cells than control mNPCs in transwell assay. B. A172-EVs-treated mNPCs had significantly more migrated cells than control mNPCs in transwell assay. C. U87-EVs-treated mNPCs showed significantly higher relative width of scratch than control mNPCs in wound-healing assay. D. A172-EVs-treated mNPCs showed significantly higher relative width of scratch than control mNPCs in wound healing assay. Results are presented as the mean ± SD of three independent experiments. **p<0.01, ***p<0.001 and ****p<0.0001, in comparison with control. Scale bar, 100 μm (A, B) and 200 μm (C, D).

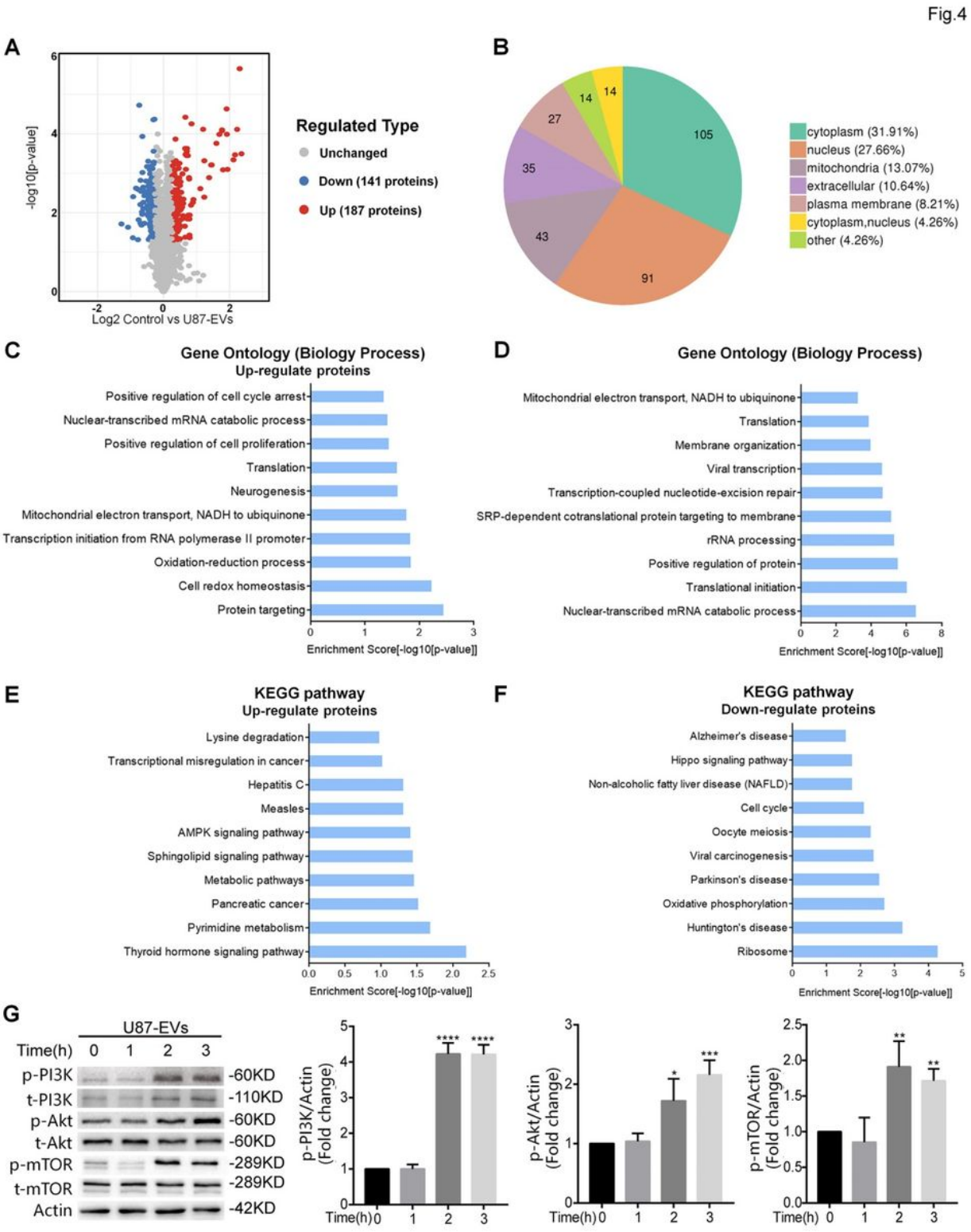

Figure 4

Proteomic analysis of U87 EVs-treated mNPCs revealed the activation of PI3K-Akt-mTOR pathway. A. Proteomic analysis revealed 187 upregulated proteins and 147 downregulated proteins in U87-EVs-treated mNPCs compared with control mNPCs. B. The distribution of changed proteins in U87-EVs-treated mNPCs. C. Top 10 biology processes of upregulated proteins revealed by Gene Ontology analysis in U87-EVs-treated mNPCs revealed. D. Top 10 biology processes of downregulated proteins in U87-EVs-treated

mNPCs revealed by Gene Ontology analysis. E. Top 10 signaling pathways of upregulated proteins in U87-EVs-treated mNPCs revealed by KEGG analysis. F. Top 10 signaling pathways of downregulated proteins in U87-EVs-treated mNPCs revealed by KEGG analysis. G. Western blot confirmation of upregulated PI3K-Akt-mTOR pathway proteins in U87-EVs-treated mNPCs. Results are presented as the mean ± SD of three independent experiments. **p<0.01, ***p<0.001 and ****p<0.0001, in comparison with 0 hour.

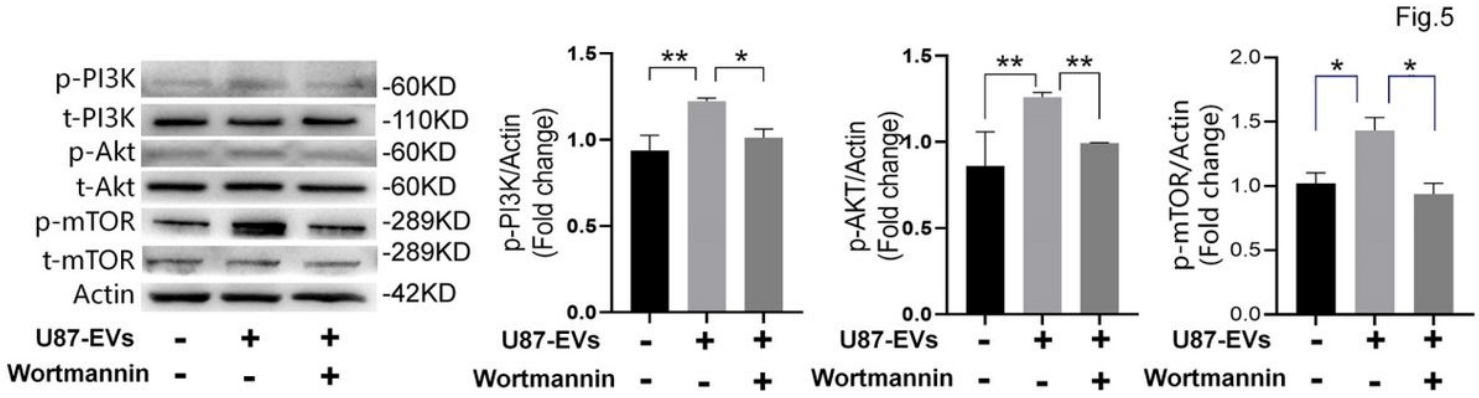

Figure 5

PI3K inhibitor Wortamnnin lowered upregulated PI3K-Akt-mTOR pathway proteins in glioblastoma-derived EVs-treated mNPCs. Western blot analysis revealed that PI3K inhibitor Wortamannin treatment lowered the protein levels of p-PI3K, p-PDK1, p-Akt, and mTOR. Results are presented as the mean ± SD of three independent experiments. *p<0.05, **p<0.01.

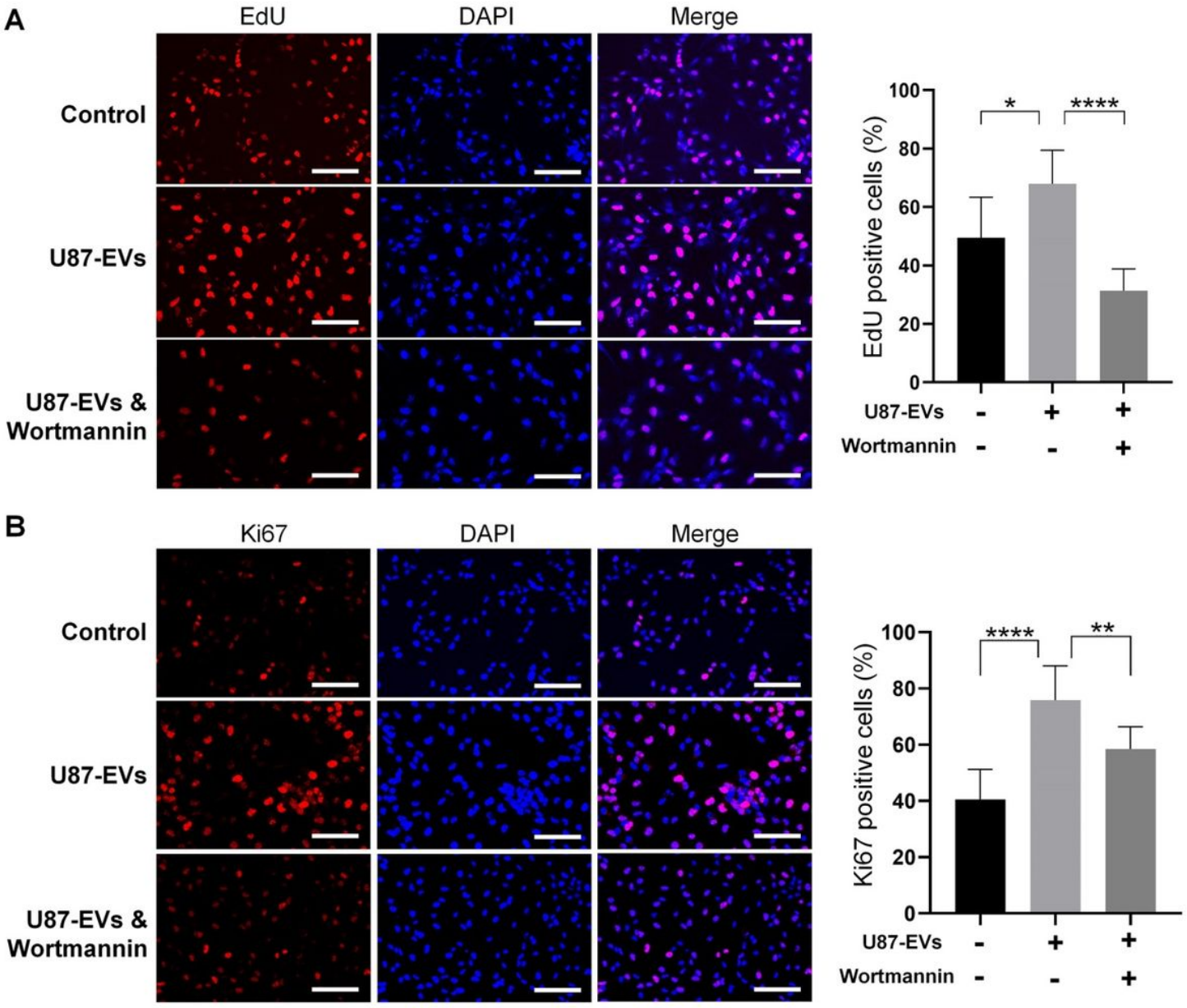

Figure 6

Inhibiting PI3K-Akt pathway in glioblastoma-derived EVs-treated mNPCs reversed elevated NPC proliferation. A. PI3K inhibitor Wortamnnin significantly reversed U87-EVs-elevated proportion of EdU-positive cells in U87-EVs-treated mNPCs. B. PI3K inhibitor Wortamnnin significantly reversed U87-EVs-elevated proportion of Ki67-positive cells in U87 EVs-treated mNPCs. Results are presented as the mean ± SD of three independent experiments. *p<0.05, **p<0.01, and ****p<0.0001. Scale bar, 50 μm.

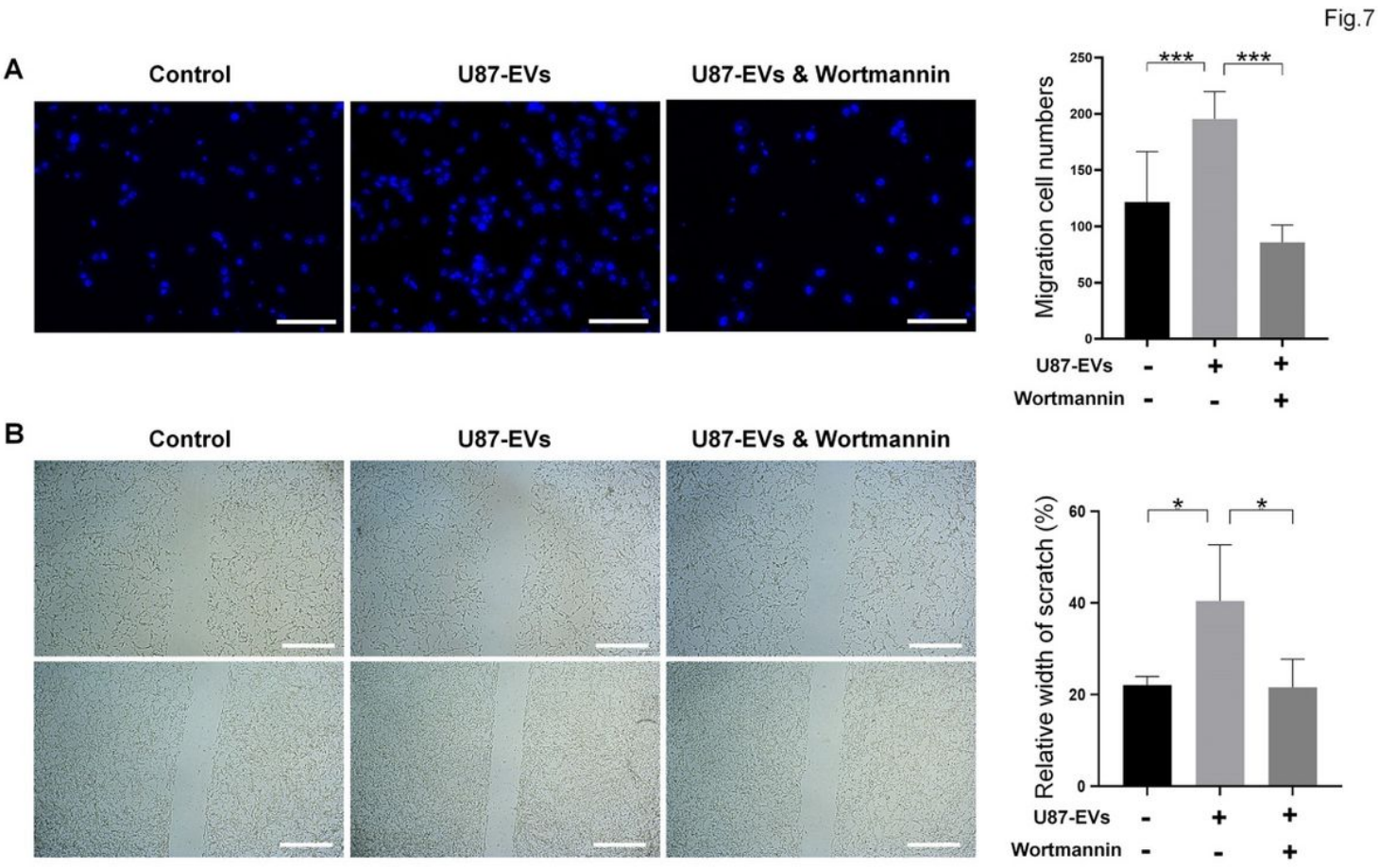

Figure 7

Inhibiting PI3K-Akt pathway in glioblastoma-derived EVs-treated mNPCs reversed elevated NPC migration. A. PI3K inhibitor Wortamnnin significantly reversed U87-EVs-elevated migration cell numbers in U87-EVs-treated mNPCs in the transwell assay. B. PI3K inhibitor Wortamnnin significantly reversed U87-EVs-elevated relative width of scratch in U87-EVs-treated mNPCs in wound healing assay. Results are presented as the mean ± SD of three independent experiments. *p<0.05, ***p<0.001. Scale bar, 100 μm (A) and 200 μm (B).

Supplementary Files

This is a list of supplementary files associated with this preprint. Click to download.

- SupplementalInformation.docx